



# Comparison of near-infrared spectroscopy and hyperspectral imaging for internal quality determination of ‘Nam Dok Mai’ mango during ripening

Parika Rungpichayapichet<sup>1</sup> · Nimmitra Chaiyarattanachote<sup>1</sup> · Pramote Khuwijitjaru<sup>1</sup> · Kyuya Nakagawa<sup>2</sup> · Marcus Nagle<sup>3</sup> · Joachim Müller<sup>4</sup> · Busarakorn Mahayothee<sup>1</sup>

Received: 3 August 2022 / Accepted: 13 November 2022 / Published online: 2 December 2022  
© The Author(s), under exclusive licence to Springer Science+Business Media, LLC, part of Springer Nature 2022

## Abstract

In this study, the potential of near-infrared spectroscopy (NIRS) and hyperspectral imaging (HSI) techniques as non-destructive methods to determine the internal quality attributes of mangoes during ripening were evaluated and compared. A total of 188 mango fruits (cv. Nam Dokmai subcv. Si Thong) were determined for firmness, total soluble solids (TSS), titratable acidity (TA), pH,  $\beta$ -carotene content, and ripening index (RPI) for 8 days. The effect of the position (shoulder, cheek, and tip) of fruit on the changes of fruit quality during ripening and the accuracy of prediction models were also investigated. Fruit spectra were acquired by NIR spectrometer at full wavelength NIR region (800–2500 nm) and HSI system at vis/NIR region (450–998 nm). Partial least square regression was used to develop calibration models using original and pre-treated spectra from both devices. In addition, multiple linear regression (MLR) models were built from specific wavelengths obtained from multifactorial analysis. Non-significant differences of all fruit quality attributes were found between positions at the initial ripening stage while the slightly lower TA and  $\beta$ -carotene content were observed at the shoulder position compared to other sections at the end of the ripening stage. However, the fruit position showed only a slight influence on the prediction performance of the calibration models. NIRS calibration models provided only slightly better prediction performances than HSI calibration models. According to the results, both NIRS and HSI showed potential for quality control in mango sorting.

**Keywords** *Mangifera indica* · Vis/NIR HSI technique · NIR spectroscopy · Spatial variation · Fruit quality ·  $\beta$ -Carotene

## Introduction

Mango (*Mangifera indica*) is a tropical fruit with a worldwide production of 54.8 million tons in 2020 [1]. Mango is a climacteric fruit that is normally harvested at the mature, unripe stage and further ripened for a few days before

consumption. Mango is highly perishable and the eating qualities of mango during the ripening period change very quickly. Therefore, monitoring the internal quality development is important [2]. In general, determinations of internal quality of fruits are performed using various destructive testing methods which inevitably cause fruits loss during assessment and therefore complete assessment inspection cannot be conducted. Recently, several non-destructive testing methods have been receiving much attention for detecting the internal quality attributes of mango including image analysis [3], acoustic method [4], and near-infrared spectroscopy (NIRS) and hyperspectral imaging (HSI).

NIRS and HSI are rapid and non-destructive techniques for determining the internal quality attributes of fruits based on the absorption of an electromagnetic wave in the wavelength region of 700–2500 nm [5, 6]. Determination of internal quality attributes of different cultivars of mangoes during ripening using NIRS and HSI has been reported [2]. Handheld instruments with a short NIR wavelength (700–1100 nm) were

✉ Busarakorn Mahayothee  
mahayothee\_b@su.ac.th

<sup>1</sup> Department of Food Technology, Faculty of Engineering and Industrial Technology, Silpakorn University, Nakhon Pathom 73000, Thailand

<sup>2</sup> Department of Chemical Engineering, Faculty of Engineering, Kyoto University, Katsura, Nishikyō-ku, Kyoto 615-8510, Japan

<sup>3</sup> Agricultural Research and Development Program, Central State University, Wilberforce, OH 45384, USA

<sup>4</sup> Institute of Agricultural Engineering, Tropics and Subtropics Group, University of Hohenheim, 70599 Stuttgart, Germany

frequently studied because of their low cost and convenience for in field applications [7, 8]. For example, Rungpichayapichet, Mahayothee, Nagle, Khuwijitjaru and Müller [8] developed NIRS models (700–1100 nm) to determine total soluble solids (TSS), titratable acidity (TA), firmness, and the ripening index using data collected from three years for ‘Nam Dok Mai’ mango. However, long-wavelength NIRS, which is mostly available in benchtop NIR spectrometers usually provided better prediction from the absorption peaks of various chemical components such as organic acids and sugars [9]. On the other hand, studies on HSI analysis of mango during ripening are quite limited. Most HSI studies focused on in field monitoring, especially for dry matter content [10, 11]. Rungpichayapichet et al. [12] mapped the changes in firmness, TSS, and TA during the ripening of mangoes using an HSI instrument in the wavelength range of 400–1000 nm.

A comparison of NIRS and HSI on the prediction of internal quality attributes of fruit, however, has been rarely investigated. Therefore, in the present study, NIRS and HSI were employed to determine the quality attributes of ‘Nam Dok Mai’ mango, which is a substantial high-price export variety of fresh mango from Thailand. The NIRS instrument was a benchtop type that measured the full wavelength (800–2500 nm), while the HSI measured visible and short NIR wavelength (450–998 nm).

## Materials and methods

### Mango samples

A total of 188 mature mango fruits (*Mangifera indica* cv. Nam Dokmai, subcv. Si Thong) with all-yellow peel harvested from four growing areas (Lopburi, Udonthani, Phitsanulok, and Sakeaw provinces, Thailand) were used in this study. Fruits were harvested during the season, from February to May with the fruit mass ranging 250–350 g and a specific gravity greater than 1.00. Samples were washed with water and then soaked in 200 ppm peroxyacetic acid solution with fruit to solution ratio at 1:2 (w/v) to reduce the surface microorganisms. After that, the fruits were air-dried and kept in a basket to ripen under ambient conditions ( $29.7 \pm 0.7$  °C and  $66.3 \pm 4.4\%$  relative humidity) for 8 days, with the arrival day set as the first day of ripening. On each ripening day, six fruits were randomly selected for NIRS and HSI measurements as well as the reference analyses.

### Non-destructive measurement

#### NIR spectral measurement

A Fourier transform near-infrared (FT-NIR) spectrometer (MPA, Bruker Optik, Leipzig, Germany) was used to acquire fruit spectra in reflectance mode in the wavelength range

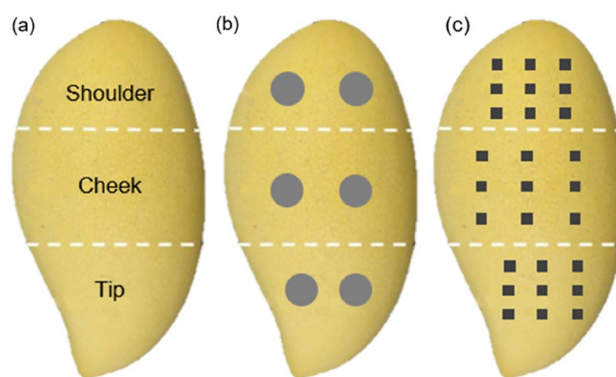


**Fig. 1** Reference analyses **a**, NIRS **b**, and HSI **c** measurement positions on ‘Nam Dok Mai’ mango fruit surface

of 800–2500 nm by averaging 32 scans at  $16 \text{ cm}^{-1}$  resolution. Spectra were collected at 25 °C from three different fruit sections assigned as shoulder, cheek, and tip as shown in Fig. 1. Average spectra from each position and average spectra from all sections were used for calibration model development. Spectral reference was automatically collected before each measurement.

#### Hyperspectral image acquisition

An HSI instrument and image acquisition in this study was set up and operated as described in our previous study [12]. Spectral data in the wavelength region between 450–998 nm were extracted from hyperspectral image files using Hyper See software (BurgerMetrics SIA, Riga, Latvia). From a total of  $910 \times 900$  pixels image, nine region of interest (ROI) areas of  $5 \times 5$  pixels were randomly marked in each fruit section (Fig. 1). Therefore, a reflectance spectrum for each fruit section was averaged from 225 pixels and was used for calibration model development.

#### Chemometrics and calibration procedure

Chemometrics and calibration model development using spectral data from both devices were performed using The Unscrambler software (version 9.7, Camo, Oslo, Norway). Spectral outliers were identified using principal component analysis (PCA) subject to Hotelling’s T-squared distribution [8]. Five different spectral pretreatment techniques namely Savitzky–Golay smoothing (SG), Savitzky–Golay first derivative (D1), Savitzky–Golay second derivative (D2) using 17 points with second-order polynomial regression, standard normal variate (SNV) transformation, and multiplicative scatter correction (MSC) were performed to improve the predictability during the development of the calibration models.

**Table 1** Descriptive statistics of 'Nam Dok Mai' mango fruit quality attributes used for calibration and validation sets in PLS modeling

	Calibration set			Validation set		
	n <sup>a</sup>	Mean	Range	n <sup>a</sup>	Mean	Range
Firmness (N)	126	14.63	5.49–30.08	62	14.60	5.78–29.43
RPI	126	3.45	0.83–7.01	62	3.44	0.99–6.74
TSS (°Brix)						
Shoulder	126	15.0	6.5–20.7	62	15.0	8.1–20.4
Cheek	126	14.4	7.6–20.4	62	14.4	6.9–21.9
Tip	126	14.7	6.9–21.9	62	14.7	7.5–20.5
Average	126	14.7	7.5–21.0	62	14.7	7.9–20.3
TA (%)						
Shoulder	126	0.66	0.04–2.73	62	0.65	0.04–2.63
Cheek	126	0.74	0.04–3.03	62	0.74	0.05–2.86
Tip	126	0.85	0.06–3.56	62	0.83	0.06–2.84
Average	126	0.75	0.05–3.10	62	0.74	0.05–2.56
pH						
Shoulder	126	4.51	2.48–6.51	62	4.51	2.53–6.26
Cheek	126	4.49	2.48–6.28	62	4.49	2.55–6.16
Tip	126	4.43	2.41–6.36	62	4.43	2.48–6.19
Average	126	4.47	2.46–6.30	62	4.48	2.53–6.15
β-carotene (mg 100 g <sup>-1</sup> )						
Shoulder	96	4.10	0.04–10.22	47	4.09	0.09–9.96
Cheek	96	5.01	0.02–12.92	47	2.01	0.11–12.41
Tip	96	4.96	0.00–13.11	47	4.93	0.00–11.95
Average	96	4.65	0.02–12.00	47	4.64	0.10–11.35

<sup>a</sup>n = number of samples

Calibration models were built using partial least square (PLS) regression. Samples were divided into calibration and validation (test) sets in the ratio 2:1 (Table 1). The physicochemical values were sorted and the samples were selected by specific intervals 'Every 2 samples counting from 3' using the Unscrambler program and the two highest and two lowest values were assigned to the calibration set. The performance of prediction models was evaluated using coefficient of determination ( $R_C^2$ ) and standard error of calibration ( $SEC$ ) and validation was evaluated based on the coefficient of prediction ( $R_V^2$ ), standard error of prediction ( $SEP$ ), bias, and the ratio of the standard deviation of the test set to  $SEP$  ( $RPD$ ).

Multiple linear regression (MLR) models were developed using specific wavelengths. Candidate variables were chosen from wavelengths which showed the relatively high absolute values in PLS regression coefficient plots and loading weight plot of the best fitting PLS model. Multifactorial analysis (backward elimination stepwise method) was used for selecting significant wavelengths. MLR calibration models were constructed using the same calibration and test set samples as PLS models.

## Reference analyses

### Firmness

Firmness was determined on the unpeeled fruit sample only at the center area of cheek position using a texture analyzer (TA-XT2i, Stable Micro Systems, Surrey, UK) because of the difficulty of measuring other positions with the instrument. A puncture test was performed using a 2 mm diameter cylindrical probe at a speed of 0.5 mm s<sup>-1</sup> and a compression depth of 10 mm. The maximum force (N) was recorded and represented the firmness of the fruit [13].

### Chemical properties

Fruits were peeled and cut into two halves. Each half was then divided into three sections (Fig. 1). Flesh from each section was cut into small pieces and homogenized (Ultra-Turrax T25 basic, IKA, Staufen, Germany). pH value was determined using a pH meter (PHM210, Radiometer Analytical SAS, Villeurbanne, France) by placing the electrode probe into the puree. Extracted juice obtained from squeezing 5 g of puree through filter cloth was used to measure TSS by a digital refractometer (PAL-1, Atago, Tokyo, Japan)

and the value was expressed as °Brix. TA was evaluated by alkaline titration with 0.1 N NaOH to a pH of 8.1 using a 100 mL dilution prepared from 5 g of puree and reported as mass percentage (%) of citric acid [14]. All measurements were done in duplicate. In addition, ripening index (RPI) was calculated from firmness (F), TSS, and TA using Eq. (1) according to Mahayothee et al. [15] to represent the ripeness of the sample.

$$\text{RPI} = \ln\left(\frac{100 \cdot F \cdot \text{TA}}{\text{TSS}}\right) \quad (1)$$

### β-Carotene content

β-Carotene was extracted from flesh via a procedure adapted from Pott et al. [16]. Approximately 5 g of homogenized flesh from each mango section was mixed with 40 mL of methanol (RCI Labscan, Bangkok, Thailand). The mixture was filtered through a sintered glass funnel. The residue was washed with methanol until colorless. The yellow-clear solution was liquid-liquid extracted with 20 mL of a mixture of acetone (RCI Labscan) and hexane (RCI Labscan) (1:1 v/v) in an amber glass separatory funnel. After separation, the hexane layer (upper phase) was firstly kept in a dark environment and the methanol layer (lower phase) was re-extracted with a mixture of acetone and hexane until colorless. Then the pooled hexane layer was washed with water to remove acetone and dried by adding 2 g of anhydrous sodium sulfate (CARLO ERBA Reagents, Milano, Italy) and 2 g of butylhydroxytoluene (BHT) (ACROS organics, Geel, Belgium) was added as an antioxidant. Hexane was evaporated using a vacuum evaporator (RV10, IKA). The residue was dissolved in isopropanol (RCI Labscan) to a volume of 10 mL and used for HPLC analysis.

The extract (20 µL) was used for quantitative analysis using an HPLC system (Shimadzu, Kyoto, Japan) as described by Rungpichayapichet et al. [17]. The separation was carried out on a reverse phase C-18 column (Inertsil ODS-3, 4.6 × 150 mm, GL Sciences, Kyoto, Japan). A mixture of methanol and acetonitrile (RCI Labscan) (7:3 v/v) was used as a mobile phase at a flow rate of 1 mL min<sup>-1</sup>. β-Carotene was detected at 450 nm using a diode array detector (SPD-M20A, Shimadzu) and a certified β-carotene (purity ≥ 95%, Sigma-Aldrich, St. Louis, MO, USA) was used to prepare a calibration curve. The β-carotene content was calculated and was expressed in mg 100 g<sup>-1</sup> (dry basis). The measurement was repeated in duplicate.

### Statistical analyses

Reference data were analyzed by analysis of variance (ANOVA) with a randomized complete block design using fruits as blocks and Duncan's multiple range test was applied

to determine significant differences between quality attributes for each fruit section with a significance level of 0.05 (SPSS version 17, Chicago, IL, USA). In addition, principal component analysis (PCA) was performed to visually examine the influence of fruit position on chemical properties i.e., TSS, TA, pH, and β-carotene content, using The Unscrambler software. The difference between actual and predicted values obtained from prediction models was analyzed by paired t-tests.

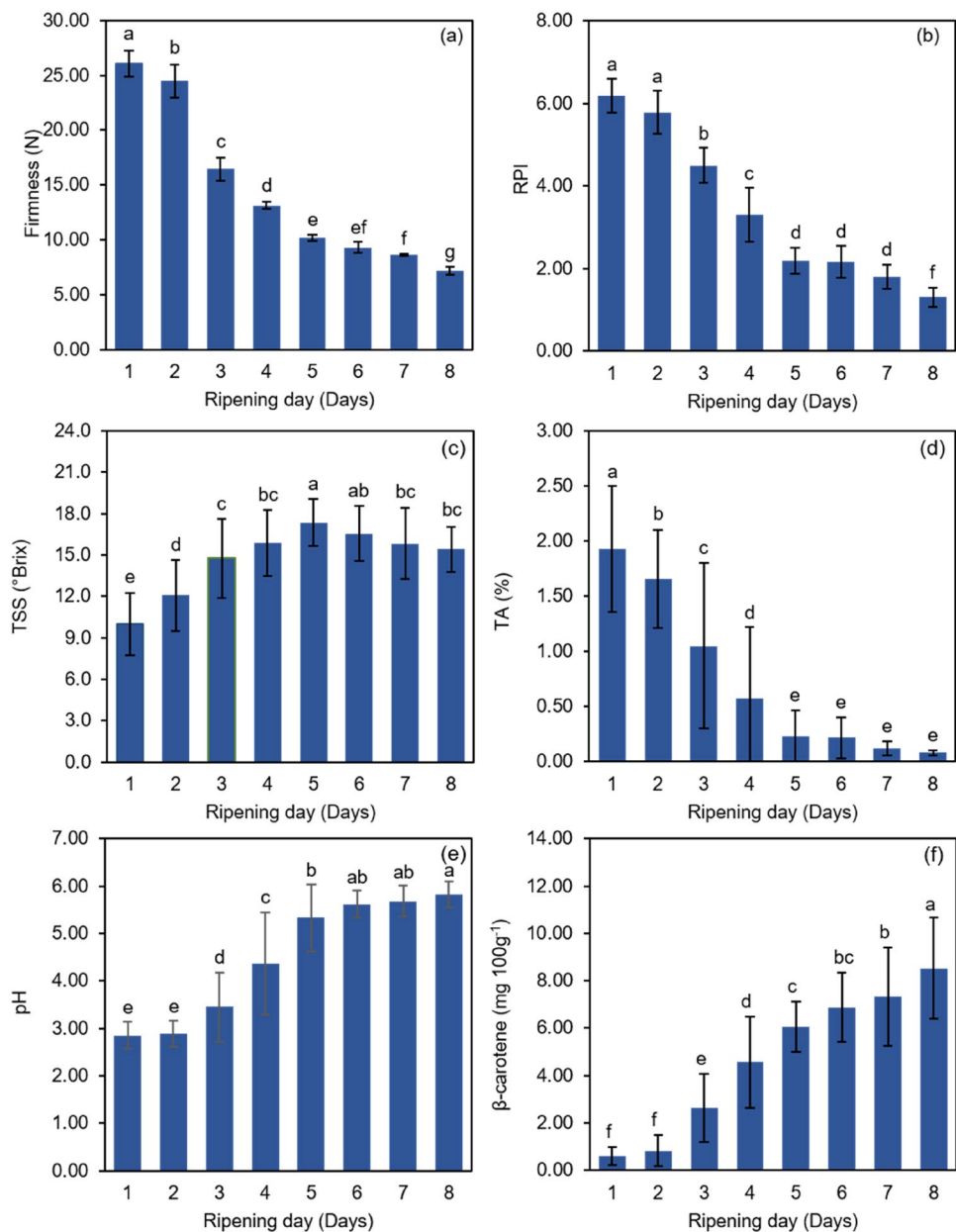
## Results and discussion

### Changes in internal quality attributes during ripening of mango

'Nam Dok Mai' mangoes used in this study were mature, unripe fruits sorted by their specific gravity higher than 1.00 [18]. The mangoes were ripened naturally at ambient temperature (29.7 ± 0.7 °C) without the addition of a ripening accelerator. Figure 2 shows the changes in important internal quality attributes, which are general ripeness indicators including TSS, TA, pH, and firmness. In addition, β-carotene content which is a major carotenoid found in mango flesh, was also determined. β-Carotene is a pro-vitamin A, which is present abundantly in mangoes. A typical ripening behavior i.e., decrease in firmness and TA, and an increase in TSS, pH, and β-carotene content was observed. Changes in the fruit quality attributes particularly occurred during the first 5 days of ripening and thereafter remained unchanged or only slightly changed to the end of the ripening period. Significant decreases (more than 60%) were found in firmness and TA during the initial ripening period, while the highest TSS value was found on the fifth day of ripening. As reported in many studies, declining firmness relates to a process of change in the cell wall structure and composition by the action of enzymes e.g., polygalacturonase, pectin methylesterase, and cellulase during ripening, while a decrease in TA is due to the degradation of acids in the respiration process. In addition, hydrolysis of starch into sugar during ripening results in a rise in TSS [19, 20]. β-Carotene content continuously increased along the ripening period, sharply increased on the third day, and reached the maximum on the last day of ripening. A similar pattern was reported in previous studies [19, 21, 22]. Compared to other cultivars, Nam Dokmai subcv. Si Thong contains higher β-carotene content (0.6–8.5 mg 100 g<sup>-1</sup>) than Haden and Ataulfo (0.4–2.8 mg 100 g<sup>-1</sup>) [2], and Tainong (1.9–3.3 mg 100 g<sup>-1</sup>) [20].

Figure 3 shows PCA scores plots of the first two principal components (PC1 and PC2) using chemical data (TA, TSS, and β-carotene content) from each mango section on days 2, 4, 6, and 8 of the ripening. Clear boundaries were not observed for data from each fruit section which indicated

**Fig. 2** Internal quality attributes of 'Nam Dok Mai' mango fruit during ripening, including **a** firmness, **b** ripening index (RPI), **c** total soluble solids (TSS), **d** titratable acidity (TA), **e** pH, and **f**  $\beta$ -carotene content. Error bars indicate standard deviation. A similar letter above the bars indicates no significant difference ( $p > 0.05$ , Duncan's test) between ripening days



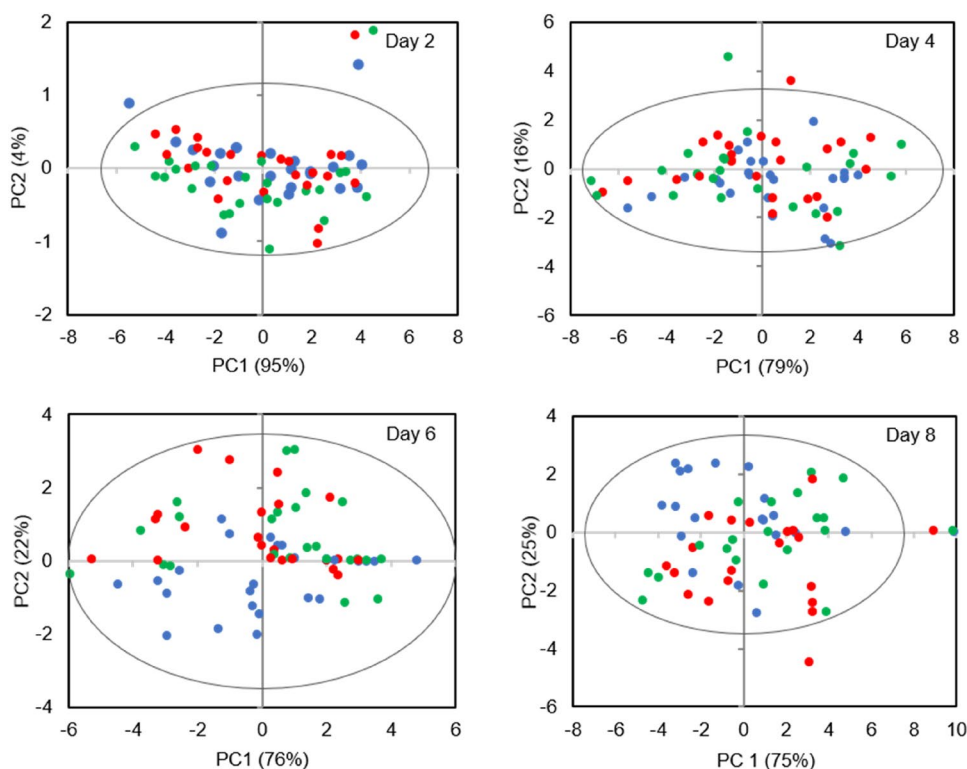
proximity of chemical compositions between fruit sections. However, in the last phase of ripening (days 6 and 8), the shoulder position was slightly distinct from other parts whereas cheek and tip positions were clustered together. This result was confirmed by ANOVA analysis (data not shown) that fruits at the shoulder position contained lower concentrations of  $\beta$ -carotene compared to cheek and tip positions on the last four days of ripening. In addition, the highest TA was found in the tip position but was not significantly different from the other parts. In a previous study [22], however, significantly higher TA in tip than cheek and shoulder were observed. The results were in contrast to Nordy et al. [23] who reported that for mango cv. Cogshall, the tip position had significantly less TA and higher TSS

than cheek and shoulder positions. However, the authors also found a non-significant difference of ethylene, a ripening related hormone, between fruit positions [23]. Therefore, non-significant variation in these fruit quality attributes in this study may be explained by this reason.

### Prediction models for physicochemical properties of mango

Postharvest changes in mango simultaneously occur in both external peel and internal pulp. These changes are regulated by ethylene content which generally accumulates in pulp closed to seed. For example, during ripening, increasing of intense yellow color can be observed in peel and pulp due

**Fig. 3** PCA score plots of ‘Nam Dok Mai’ mango on different ripening days using chemical properties including TA, TSS, and  $\beta$ -carotene content from shoulder (blue dot), cheek (red dot) and tip (green dot) positions. Ellipsis indicates the 95% confidence intervals (Color figure online)



to the carotenoid synthesis and accumulation. Degradation of protopectin to pectin results in fruit pulp softening and peel hardness as well as respiratory water loss. Therefore, internal changes in pulp often reflect changes in external peel. Postharvest changes are related to the alteration of chemical compositions which mostly consist of C, H, O in their structures, therefore these will affect to the absorption energy and spectroscopic signal. Average original spectra of mango from each day of the ripening measured by NIRS (800–2500 nm) and HSI (450–998 nm) are illustrated together in Fig. 4a. In the visible wavelength region (450–700 nm), a strong absorption was found in the blue-green light area (450–500 nm), which is associated with the presence of carotenoid compounds [24, 25]. The absence of absorption peak around 670–695 nm, which is related to the chlorophylls, might be attributed to the characteristic all-yellow peel of this mango cultivar [26]. Broad band absorption peaks at 900–1050, 1100–1300, 1400–1600, and 1900–2000 nm were observed in the NIR region. These absorption bands are associated with the absorptions of C–H and O–H bonds in water and organic matters such as sugar, acids, and  $\beta$ -carotene [25, 27, 28]. As can be seen on the spectra, there were baseline shifts and overlapping peaks which might have affected the prediction performance, therefore the spectra were adjusted prior to calibration model development using several spectral pretreatment techniques.

Both original and pretreated spectra obtained from NIRS and HSI were used to develop calibration models for

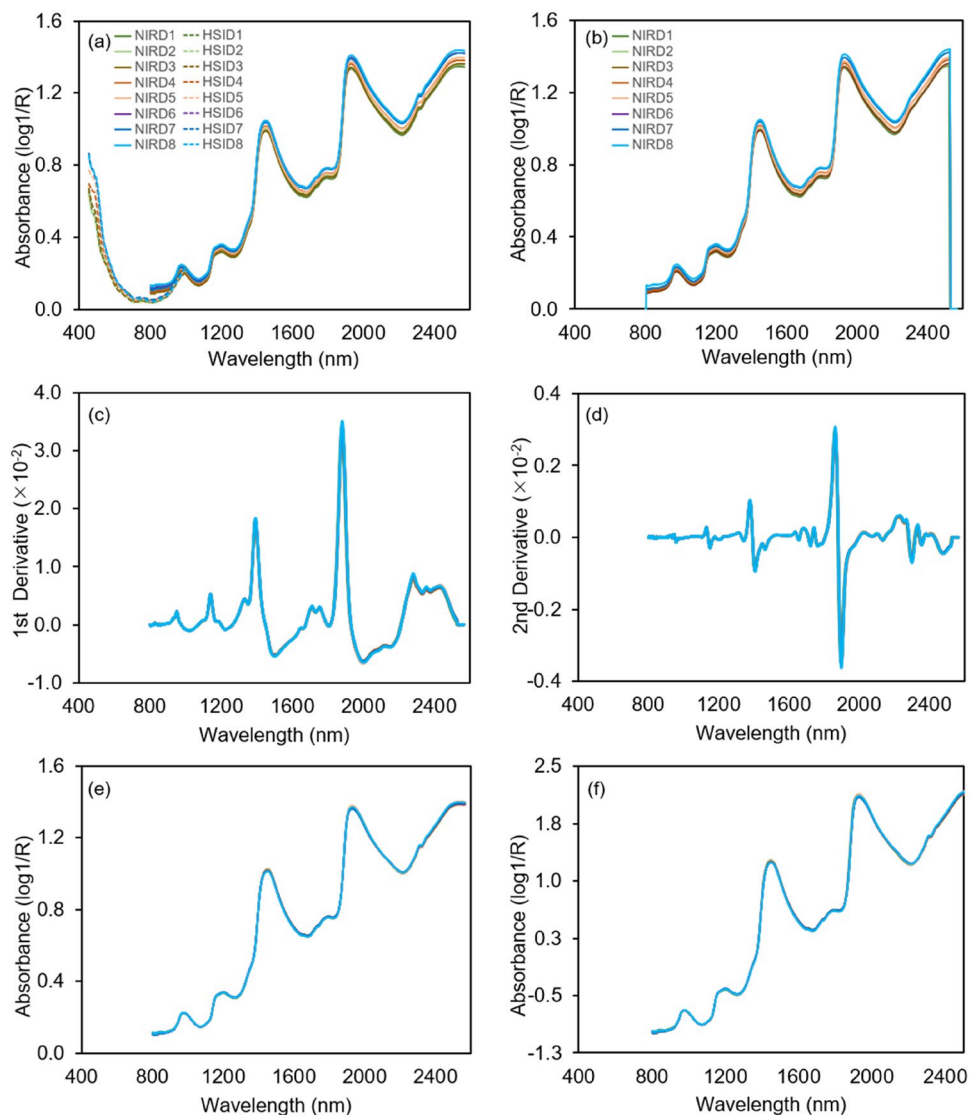
firmness, TSS, TA, pH, RPI, and  $\beta$ -carotene content. Several spectral pretreatment techniques including Savitzky-Golay smoothing (second polynomial order, 17 point), Savitzky-Golay first derivative (second polynomial order, 17 point), Savitzky-Golay second derivative (second polynomial order, 17 point), standard normal variate (SNV), and multiplicative scatter correction (MSC) were applied to adjust the spectral resolution (Fig. 4b–f).

### NIRS prediction models

The best PLS regression results for the prediction of mango quality in each fruit section using NIR spectra are shown in Table 2. The best prediction ability for fruit quality attributes was obtained from the model developed from average fruit spectra, which were pretreated with D1, MSC and SNV. MSC and SNV techniques are known as the methods used to remove the effects of scattering and reduce baseline shift which can improve the spectral resolution [24, 28, 29]. However, TA was most accurately predicted by using the model developed from D2 pretreatment. The maximum *RPD* was found for RPI model at 3.16 with *SEP* of 0.54. However, less prediction ability was observed on the TSS model with  $R_C^2$ , *SEP* and *RPD* ranging between 0.78 and 0.93, 1.22–1.69 °Brix and 1.83–2.64, respectively.

Regarding the fruit position, the calibration model developed from the tip position spectra showed a lower

**Fig. 4** Average spectra of ‘Nam Dok Mai’ mango during ripening **a** original NIRS (solid line) and HSI (dash line) spectra, **b** SG-NIRS spectra, **c** D1-NIRS spectra, **d** D2-NIRS spectra, **e** MSC-NIRS spectra, and **f** SNV-NIRS spectra



prediction error for all quality attributes. Based on the  $R_V^2$  and  $RPD$  values, the prediction model for pH shows the best predicting performance ( $R_V^2 = 0.90$ ,  $RPD = 3.11$ ) followed by those for TA ( $R_V^2 = 0.86$ ,  $RPD = 2.70$ ), and TSS ( $R_V^2 = 0.83$ ,  $RPD = 2.46$ ). In this study,  $RPD$  values obtained from NIRS prediction models were in a range of 1.83–3.16. Munawar, Zulfahrizal, Meilina and Pawelzik [28] suggested that for quantitative prediction. Models with an  $RPD$  value between 2 and 2.5 are acceptable, while an  $RPD$  value between 2.5 and 3 or above indicates a good and excellent prediction accuracy. Therefore, the prediction models for all mango quality attributes developed from NIRS average spectra in this study are promising. Similar result was reported by Xu, Xu, Xie and Ying [30] that prediction models of soluble solids content (SSC) developed from the average spectra obtained from

7 different positions of apple fruits provided the accurate prediction performance.

### HSI prediction models

Table 3 shows the best PLS regression results for the prediction of mango quality in each fruit section using HSI spectra. Similar to the NIRS regression results, calibration models developed from average spectra showed the best prediction performance in all fruit attributes except for pH, which the model developed from cheek spectra provided the best prediction ability. Overall, slightly lower accuracy of HSI prediction models as compared to NIRS prediction models, which might be because only absorbance data in visible and short-wavelength regions were measured. The best-fitting regression for firmness was achieved from SG pretreated spectra with  $R_C^2$ ,  $SEP$ , and  $RPD$  of 0.81, 2.62 N,

**Table 2** NIRS-PLS regression results for ‘Nam Dok Mai’ mango fruit quality attributes in different sections

	Pretreatment	<i>F</i>	<i>RPD</i>	Calibration		Validation		
				$R_C^2$	<i>SEC</i>	$R_V^2$	<i>SEP</i>	Bias
Firmness (N)	D1	10	2.57	0.87	2.62	0.84	2.80	0.73
RPI	D1	9	3.16	0.91	0.59	0.90	0.61	-0.01
TSS (°Brix)								
Shoulder	MSC	8	2.23	0.78	1.5	0.80	1.4	0.1
Cheek	D1	10	1.83	0.89	1.1	0.69	1.7	0.3
Tip	MSC	10	2.46	0.87	1.3	0.83	1.4	0.1
Average	D2	9	2.64	0.93	0.9	0.85	1.2	-0.3
TA (%)								
Shoulder	MSC	10	2.26	0.84	0.31	0.80	0.33	0.01
Cheek	None	10	2.12	0.83	0.35	0.77	0.39	-0.08
Tip	MSC	9	2.70	0.87	0.32	0.86	0.33	-0.04
Average	D2	9	3.07	0.90	0.26	0.89	0.26	0.07
pH								
Shoulder	SNV	8	2.55	0.84	0.53	0.85	0.53	0.00
Cheek	SNV	9	3.02	0.87	0.47	0.89	0.43	-0.05
Tip	SNV	10	3.11	0.92	0.40	0.90	0.44	0.00
Average	D1	10	2.99	0.93	0.35	0.88	0.45	-0.12
$\beta$ -carotene (mg 100 g <sup>-1</sup> )								
Shoulder	MSC	10	1.93	0.88	0.99	0.73	1.42	-0.03
Cheek	SNV	7	2.43	0.84	1.41	0.82	1.41	-0.29
Tip	MSC	10	2.34	0.86	1.35	0.80	1.48	-0.45
Average	MSC	10	2.65	0.89	1.08	0.86	1.19	0.10

*SG* Savitzky-Golay smoothing, *D1* Savitzky-Golay first derivative, *D2* Savitzky-Golay second derivative, *SNV* standard normal variate, *MSC* multiplicative scatter correction, *F* number of factors

and 2.75, respectively. Screening quantitative prediction performance (*RPD* between 1.5 and 1.9) was observed for the TSS calibration model. The results agreed with many researchers that HSI has lower prediction performance for TSS than other attributes, e.g. firmness [12, 31, 32]. This might be because HSI relies on the scattering effect and the visible range wavelength included in HSI measurement does not enhance the predicting ability for TSS [31]. A relatively good prediction of  $\beta$ -carotene content was obtained from SNV pretreated spectra with  $R_C^2$ , *SEP*, and *RPD* of 0.84, 1.13 mg 100 g<sup>-1</sup>, and 2.80, respectively. The better prediction accuracy on  $\beta$ -carotene content using HSI spectra compared to NIRS might be attributed to high absorption in the visible wavelength region around 450–500 nm.

Scatter plots of the best calibration results for predicting mango fruit attributes using NIRS and HSI techniques are illustrated in Figs. 5 and 6. Based on the paired t-test methods, for all calibration models, no significant differences ( $p > 0.05$ ) between actual and predicted quality attributes were found from both techniques (data not shown).

## MLR calibration models

To identify the relevant wavelengths that are important to estimate each mango quality parameter, loading weight value and PLS regression coefficient were computed and analyzed. Figure 7 shows an example of NIRS-PLS regression coefficient and loading weight plot, which represent relevant variables for TSS prediction. Significantly contributed variables were mainly located in the long-wavelength region (1100–2500 nm). A set of wavelengths representing the first overtone of O–H absorptions and C–H combinations (1350–1450 nm), the first overtone of C–H bond (1600–1800 nm) and the region between 2100 and 2400 nm that corresponded to water and carbohydrate absorption was observed as relevant wavelengths for TSS prediction. For firmness prediction models, the second overtone of the C=O bond (1800–1900 nm) and combinations of C–H + C–H absorption (2200–2400 nm) were found as relevant variables. The results were in agreement with Buyukcan and Kavdir [33] that the effective wavelength ranges for SSC of apricot were between 1333 and 1836 nm and between 2173 and 2300 nm while the effective wavelength ranges for firmness were between 800 and 1836 nm and between 2173



**Table 3** HSI-PLS regression results for 'Nam Dok Mai' mango fruit quality attributes in different sections

	Pretreatment	<i>F</i>	<i>RPD</i>	Calibration		Validation		
				$R_C^2$	<i>SEC</i>	$R_V^2$	<i>SEP</i>	Bias
Firmness (N)	SG	4	2.75	0.81	3.14	0.87	2.62	0.24
RPI	None	4	3.17	0.90	0.63	0.90	0.61	-0.03
TSS (°Brix)								
Shoulder	SG	6	1.60	0.56	2.1	0.59	2.0	0.4
Cheek	SG	10	1.47	0.72	1.7	0.52	2.1	0.4
Tip	MSC	4	1.52	0.57	2.4	0.56	2.3	0.3
Average	SG	9	1.78	0.58	2.1	0.69	1.8	0.0
TA (%)								
Shoulder	D2	2	2.50	0.79	0.35	0.84	0.30	0.00
Cheek	MSC	8	2.34	0.88	0.29	0.81	0.35	-0.08
Tip	D2	2	2.51	0.85	0.35	0.84	0.36	-0.03
Average	D2	3	2.69	0.86	0.31	0.86	0.30	0.05
pH								
Shoulder	D1	2	2.98	0.88	0.46	0.89	0.45	0.00
Cheek	SNV	7	3.65	0.93	0.35	0.92	0.36	0.10
Tip	SNV	5	3.02	0.90	0.44	0.88	0.45	0.13
Average	None	8	3.58	0.94	0.34	0.92	0.37	-0.01
$\beta$ -carotene (mg 100 g <sup>-1</sup> )								
Shoulder	D2	3	2.09	0.81	1.20	0.77	1.31	0.11
Cheek	D2	2	2.35	0.84	1.41	0.82	1.46	-0.20
Tip	SG	6	2.36	0.82	1.54	0.82	1.49	-0.11
Average	SNV	4	2.80	0.84	1.30	0.87	1.13	0.10

SG Savitzky-Golay smoothing, D1 Savitzky-Golay first derivative, D2 Savitzky-Golay second derivative, SNV standard normal variate, MSC multiplicative scatter correction, *F* number of factors

and 2355 nm. Similar to firmness and TSS models, a set of wavelengths around 1700 and 2200–2400 nm was observed in the  $\beta$ -carotene content prediction model.

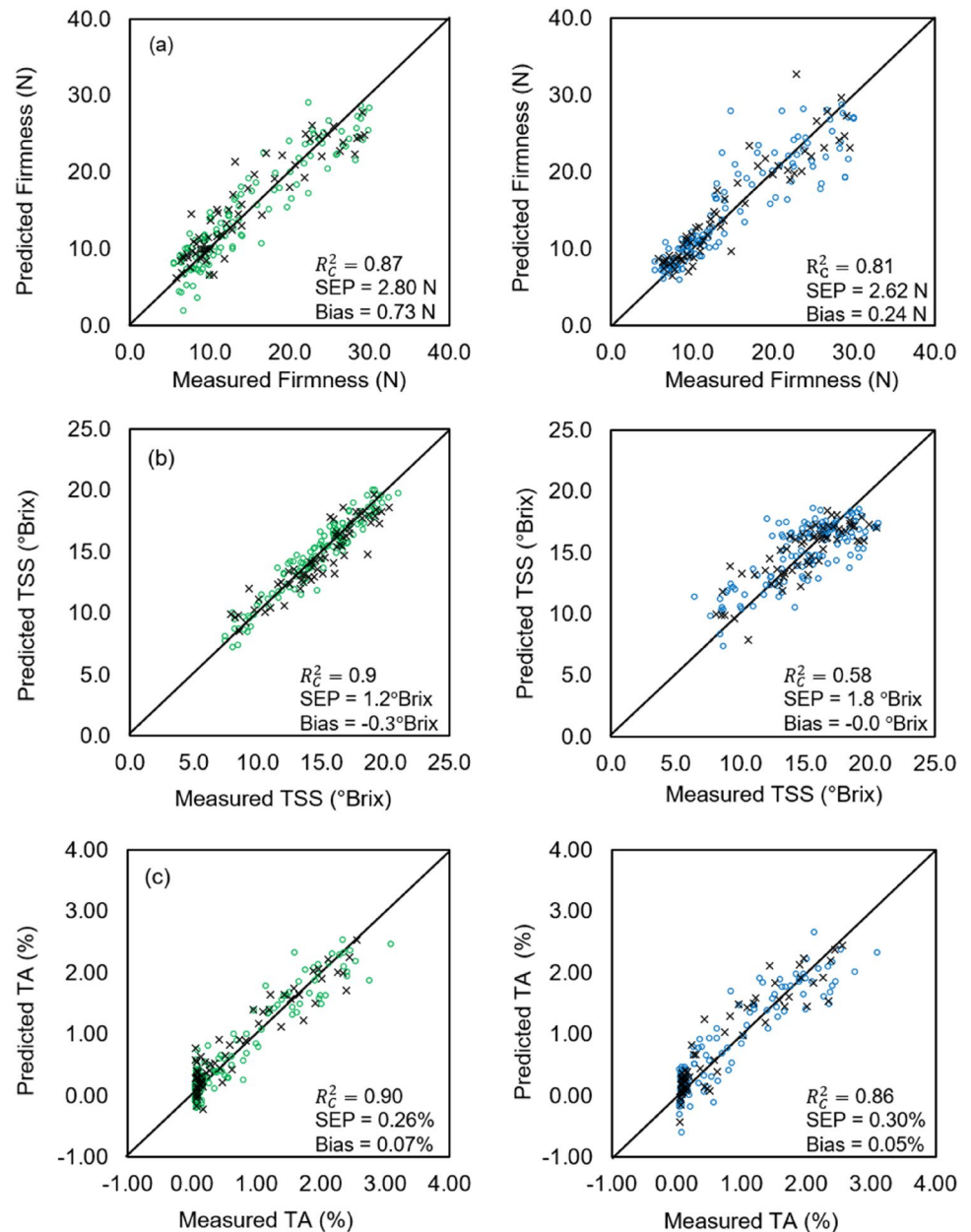
From the regression coefficient plot and loading weight plot of the best fitting PLS prediction models, the relevant wavelengths were chosen as candidate wavelengths and evaluated for significant impact using the backward elimination stepwise method and the number of significant wavelengths used for NIRS-MLR model construction were defined as describe in our previous study [17]. Table 4 shows prediction performance of NIRS-MLR prediction models developed by significant wavelengths. Lower predictive accuracy was observed on MLR models compared to PLS model due to a smaller number of variables used for model construction. The minimum number of wavelengths was found for firmness model at three wavelengths, 2310, 2344, and 2400 nm, whereas pH (1692, 1719, 1730, and 2396 nm) and  $\beta$ -carotene content prediction model (1721, 1735, 2212, and 2314 nm) required four significant wavelengths. Five significant variables (1350, 1392, 1878, 1931, and 1997 nm) were used for RPI prediction model while greater number of variables were chosen for TSS (7 wavelengths including 1402, 1418,

1668, 1687, 1705, 1733, and 2031 nm) and TA prediction model (1145, 1161, 1673, 1688, 1708, 1735, and 1752 nm).

PLS regression coefficient plots of TA, pH, and  $\beta$ -carotene content prediction developed from average HSI spectra are illustrated in Fig. 8. Candidate variables were selected and evaluated by the backward elimination stepwise method. Prediction results of HSI-MLR models developed using significant wavelengths are listed in Table 5. For HSI-MLR prediction models, the important wavelengths for TA determination were 514, 550, 646, 710, 886, and 890 nm. This set of wavelengths represented the fourth overtone (710 nm) and the third overtone (890 nm) of C-H bonds and carotenoids absorption. For pH prediction, four wavelengths (482, 514, 550, and 802 nm) were included in the MLR prediction model. These results agreed with the finding of other studies, which showed that the spectral regions at visible wavelengths are capable to predict TA and pH [34, 35]. However, the ability of visible wavelength to determine pH might be from the relation between the changes of pigments and internal fruit quality attributes during fruit ripening [36].

For  $\beta$ -carotene content prediction, important wavelengths were 466, 482, 518, 546, 578, 678, 922, and 954 nm. As reported by Davey et al. [37], a wavelength

**Fig. 5** Prediction results for **a** firmness, **b** total soluble solids (TSS), **c** titratable acidity (TA) of ‘Nam Dok Mai’ mango using NIRS calibration models (green color) and HSI calibration models (blue color) (open circle calibration set, × validation set) (Color figure online)

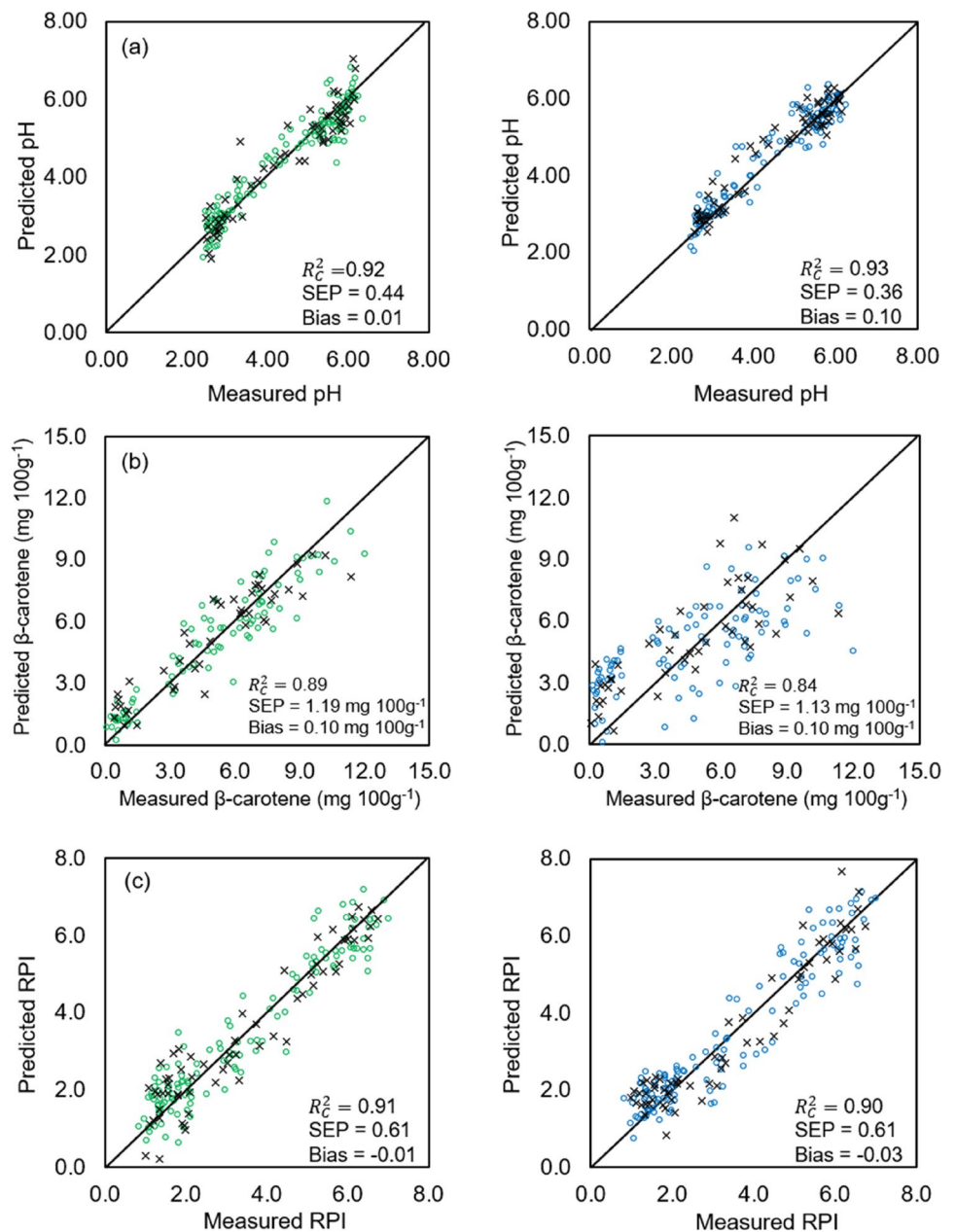


region between 400 and 600 nm is strongly absorbed by carotenoids, especially at 520 and 540 nm. Therefore, a greater number of wavelengths around 450–600 nm were found as the important wavelengths that enhance the predicting ability of the  $\beta$ -carotene content prediction model. Four significant wavelengths, 514, 554, 674, and 914 nm, were responsible for firmness prediction while five variables were required for RPI (514, 524, 678, 858, and 990 nm) and TSS prediction models (506, 538, 671, 762, and 898 nm).

## Conclusion

This study was performed to explore the potential of NIRS and HSI as non-destructive techniques for internal quality attributes assessment of mangoes. Fruit position showed only a slight influence on the prediction performance for both devices, and using the average fruit spectra gave the best prediction performance. The PLS models developed from NIRS spectra provided an acceptable and good prediction ability for firmness ( $RPD = 2.57$ ),

**Fig. 6** Prediction results for **a** pH, **b**  $\beta$ -carotene content, and **c** RPI of 'Nam Dok Mai' mango using NIRS calibration models (green color) and HSI calibration models (blue color) (open circle calibration set,  $\times$  validation set) (Color figure online)



TSS ( $RPD = 1.83$ – $2.64$ ), TA ( $RPD = 2.12$ – $3.07$ ), pH ( $RPD = 2.55$ – $3.11$ ), RPI ( $RPD = 3.16$ ), and  $\beta$ -carotene content ( $RPD = 1.93$ – $2.65$ ). Slightly lower prediction accuracy was found for the models obtained from HSI spectra with the  $RPD$  ranging between 1.47 and 3.58. Although the reduction of variable numbers in MLR prediction models resulted in slightly lower prediction ability of the models from both devices, acceptable prediction performances

for general screening purposes were obtained. The overall results obtained in this study showed the feasibility of NIRS and HSI for quality control in mango sorting. However, this study was performed using mango from one cultivar therefore further study is still required involving analysis of more samples from different harvest years or other cultivars.

**Fig. 7** Regression coefficient plot and loading weight plot for TSS prediction developed from average ‘Nam Dok Mai’ mango fruit spectra measured by NIRS

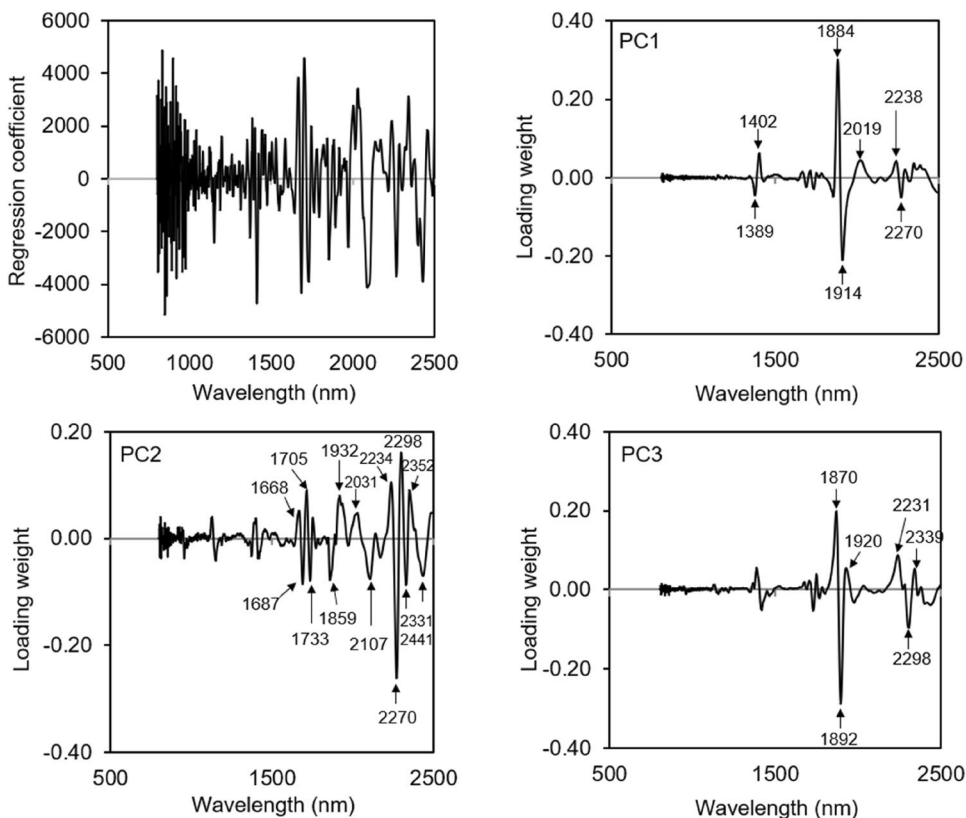


**Table 4** NIRS-MLR prediction results for ‘Nam Dok Mai’ mango fruit quality attributes

	Pretreatment	N	RPD	Calibration		Validation		
				$R_C^2$	SEC	$R_V^2$	SEP	Bias
Firmness (N)	None	3	1.71	0.66	4.25	0.66	4.20	- 0.05
RPI	None	5	1.74	0.78	0.92	0.68	1.11	- 0.14
TSS (°Brix)	None	7	2.14	0.83	1.37	0.78	1.50	- 0.10
TA (%)	None	7	2.29	0.75	0.41	0.81	0.35	0.07
pH	SNV	4	2.07	0.80	0.61	0.77	0.66	- 0.02
$\beta$ -carotene (mg 100 g <sup>-1</sup> )	MSC	4	1.63	0.63	1.96	0.64	1.94	0.34

SNV standard normal variate, MSC multiplicative scatter correction, N number of significant wavelengths

**Table 5** HSI-MLR prediction results for ‘Nam Dok Mai’ mango fruit quality attributes

	Pretreatment	N	RPD	Calibration		Validation		
				$R_C^2$	SEC	$R_V^2$	SEP	Bias
Firmness (N)	None	4	2.69	0.82	3.10	0.86	2.68	0.03
RPI	None	5	3.10	0.89	0.64	0.90	0.62	0.01
TSS (°Brix)	None	5	1.69	0.54	2.21	0.65	1.85	0.00
TA (%)	None	6	2.33	0.85	0.32	0.83	0.34	0.04
pH	None	4	3.08	0.91	0.39	0.90	0.43	0.02
$\beta$ -carotene (mg 100 g <sup>-1</sup> )	None	8	2.64	0.86	1.22	0.87	1.20	0.13

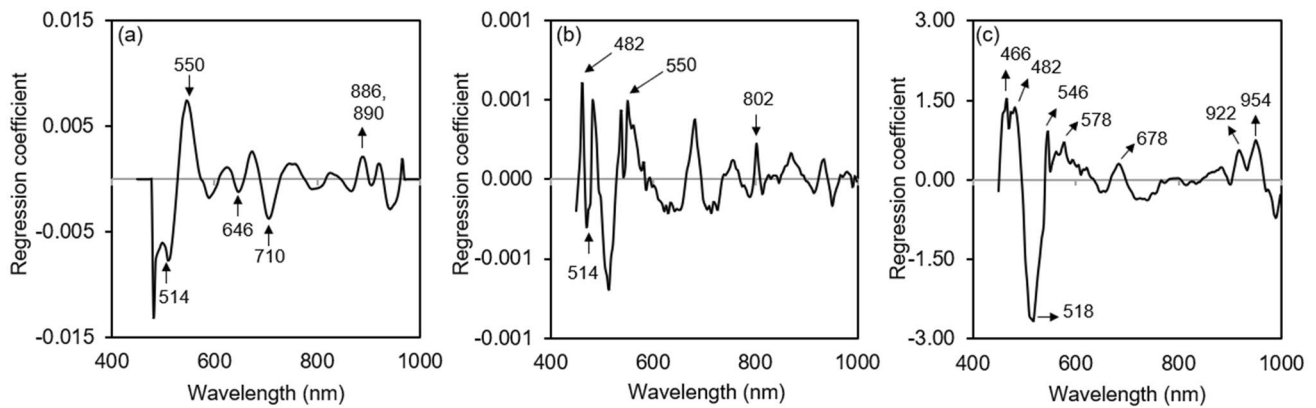


**Fig. 8** Regression coefficient plots for **a** TA **b** pH, and **c**  $\beta$ -carotene content prediction developed from average ‘Nam Dok Mai’ mango fruit spectra measured by HSI

**Acknowledgements** The hyperspectral equipment was provided by the SFB 564 project T4 funded by Deutsche Forschungsgemeinschaft (DFG), Germany.

**Author contributions** Conceptualization, PR, NC, MN and BM; Methodology, NC, MN and BM; Formal analysis, PR, NC and PK; Investigation, MN; Re-sources, MN, JM and BM; Data curation, PK and BM; Writing—original draft preparation, PR and PK Writing—review and editing, PR, NC, PK, KN MN, JM and BM; Supervision, BM; Funding acquisition, PK, KN, and BM.

**Funding** Financial support from Reinventing University System Program by the Ministry of Higher Education. Science, Research and Innovation is gratefully acknowledged (Fiscal Year 2021).

**Data availability** Research data are available from the corresponding author upon request.

## Declarations

**Conflict of interest** The authors declare no conflict of interest.

**Informed consent** Not applicable.

**Institutional review board statement** Not applicable.

## References

1. FAO, *Food and Agriculture Data - FAOSTAT* (2022)
2. M.L. Ntsoane, M. Zude-Sasse, P. Mahajan, D. Sivakumar, Quality assessment and postharvest technology of mango: a review of its current status and future perspectives. *Sci. Hort.* **249**, 77–85 (2019)
3. M. Shamili, The estimation of mango fruit total soluble solids using image processing technique. *Sci. Hort.* **249**, 383–389 (2019)
4. N. Arai, M. Miyake, K. Yamamoto, I. Kajiwara, N. Hosoya, Soft mango firmness assessment based on Rayleigh waves generated by a laser-induced plasma shock wave technique. *Foods* **10**(2), 323 (2021).
5. M. Manley, Near-infrared spectroscopy and hyperspectral imaging: non-destructive analysis of biological materials. *Chem. Soc. Rev.* **43**(24), 8200–8214 (2014)
6. H. Wang, J. Peng, C. Xie, Y. Bao, Y. He, Fruit quality evaluation using spectroscopy technology: a review. *Sensors* **15**(5), 11889–11927 (2015)
7. P. Mishra, E. Woltering, N. El Harchioui, Improved prediction of ‘Kent’ mango firmness during ripening by near-infrared spectroscopy supported by interval partial least square regression. *Infrared Phys. Technol.* **110**, 103459 (2020)
8. P. Rungpichayapichet, B. Mahayothee, M. Nagle, P. Khuwijitjaru, J. Müller, Robust NIRS models for non-destructive prediction of postharvest fruit ripeness and quality in mango. *Postharvest Biol. Technol.* **111**, 31–40 (2016)
9. T. Nordey, J. Joas, F. Davrieux, M. Chillet, M. Léchaudel, Robust NIRS models for non-destructive prediction of mango internal quality. *Sci. Hort.* **216**, 51–57 (2017)
10. S. Gutiérrez, A. Wendel, J. Underwood, Spectral filter design based on in-field hyperspectral imaging and machine learning for mango ripeness estimation. *Comput. Electron. Agric.* **164**, 104890 (2019)
11. A. Wendel, J. Underwood, K. Walsh, Maturity estimation of mangoes using hyperspectral imaging from a ground based mobile platform. *Comput. Electron. Agric.* **155**, 298–313 (2018)
12. P. Rungpichayapichet, M. Nagle, P. Yuwanbun, P. Khuwijitjaru, B. Mahayothee, J. Müller, Prediction mapping of physicochemical properties in mango by hyperspectral imaging. *Biosyst. Eng.* **159**, 109–120 (2017)
13. S.N. Jha, A.R.P. Kingsly, S. Chopra, Physical and mechanical properties of mango during growth and storage for determination of maturity. *J. Food Eng.* **72**(1), 73–76 (2006)
14. AOAC, *Official Methods of Analysis of AOAC International*, 17th edn. (AOAC International, Maryland, 2000)
15. B. Mahayothee, S. Neidhart, R. Carle, W. Mühlbauer, Effects of variety, ripening condition and ripening stage on the quality of sulphite-free dried mango slices. *Eur. Food Res. Technol.* **225**(5), 723–732 (2007)
16. I. Pott, M. Marx, S. Neidhart, W. Mühlbauer, R. Carle, Quantitative determination of  $\beta$ -carotene stereoisomers in fresh, dried, and solar-dried mangoes (*Mangifera indica* L.). *J. Agric. Food Chem.* **51**(16), 4527–4531 (2003)
17. P. Rungpichayapichet, B. Mahayothee, P. Khuwijitjaru, M. Nagle, J. Müller, Non-destructive determination of  $\beta$ -carotene content in mango by near-infrared spectroscopy compared with colorimetric measurements. *J. Food Compos. Anal.* **38**, 32–41 (2015)

18. B. Jarimopas, U. Kitthawee, Firmness properties of mangoes. *Int. J. Food Prop.* **10**(4), 899–909 (2007)
19. S. Liu, H. Huang, D.J. Huber, Y. Pan, X. Shi, Z. Zhang, Delay of ripening and softening in ‘Guifei’ mango fruit by postharvest application of melatonin. *Postharvest Biol. Technol.* **163**, 111136 (2020)
20. K. Hu, D. Peng, L. Wang, H. Liu, B. Xie, Z. Sun, Effect of mild high hydrostatic pressure treatments on physiological and physicochemical characteristics and carotenoid biosynthesis in postharvest mango. *Postharvest Biol. Technol.* **172**, 111381 (2021)
21. P.P.S. Gill, S.K. Jawandha, N. Kaur, N. Singh, Physico-chemical changes during progressive ripening of mango (*Mangifera indica* L.) cv. Dashehari under different temperature regimes. *J. Food Sci. Technol.* **54**(7), 1964–1970 (2017)
22. B. Mahayothee, P. Rungpichayapichet, P. Yuwanbun, P. Khuwijitaru, M. Nagle, J. Müller, Temporal changes in the spatial distribution of physicochemical properties during postharvest ripening of mango fruit. *J. Food Meas. Charact.* **14**(2), 992–1001 (2020)
23. T. Nordey, M. Léchaudel, M. Génard, J. Joas, Spatial and temporal variations in mango colour, acidity, and sweetness in relation to temperature and ethylene gradients within the fruit. *J. Plant Physiol.* **171**(17), 1555–1563 (2014)
24. A. Arruda de Brito, F. Campos, A. dos Reis Nascimento, C. Damiani, F. Alves da Silva, G.H. de Almeida Teixeira, L.C. Cunha Júnior, Non-destructive determination of color, titratable acidity, and dry matter in intact tomatoes using a portable Vis-NIR spectrometer. *J. Food Compos. Anal.* **107**, 104288 (2022)
25. K.B. Walsh, J. Blasco, M. Zude-Sasse, X. Sun, Visible-NIR ‘point’ spectroscopy in postharvest fruit and vegetable assessment: the science behind three decades of commercial use. *Postharvest Biol. Technol.* **168**, 111246 (2020)
26. D.S. Kasampalis, P. Tsouvaltzis, K. Ntouros, A. Gertsis, I. Gitas, A.S. Siomos, The use of digital imaging, chlorophyll fluorescence and Vis/NIR spectroscopy in assessing the ripening stage and freshness status of bell pepper fruit. *Comput. Electron. Agric.* **187**, 106265 (2021)
27. L. Feng, M. Zhang, B. Adhikari, Z. Guo, Nondestructive detection of postharvest quality of cherry tomatoes using a portable NIR spectrometer and chemometric algorithms. *Food. Anal. Methods* **12**(4), 914–925 (2019)
28. A.A. Munawar, Zulfahrizal, H. Meilina, E. Pawelzik, Near-infrared spectroscopy as a fast and non-destructive technique for total acidity prediction of intact mango: comparison among regression approaches. *Comput. Electron. Agric.* **193**, 106657 (2022)
29. Z. Wang, S.W. Erasmus, X. Liu, S.M. van Ruth, Study on the relations between hyperspectral images of bananas (*Musa* spp.) from different countries, their compositional traits and growing conditions. *Sensors* **20**(20), 5793 (2020)
30. X. Xiao, X. Huirong, X. Lijuan, Y. Yibin, Effect of measurement position on prediction of apple soluble solids content (SSC) by an on-line near-infrared (NIR) system. *J. Food Meas. Charact.* **13**, 506–512 (2019)
31. G.A. Leiva-Valenzuela, R. Lu, J.M. Aguilera, Prediction of firmness and soluble solids content of blueberries using hyperspectral reflectance imaging. *J. Food Eng.* **115**(1), 91–98 (2013)
32. P. Rajkumar, N. Wang, G. Eimasry, G.S.V. Raghavan, Y. Garipey, Studies on banana fruit quality and maturity stages using hyperspectral imaging. *J. Food Eng.* **108**(1), 194–200 (2012)
33. M.B. Buyukcan, I. Kadir, Prediction of some internal quality parameters of apricot using FT-NIR spectroscopy. *J. Food Meas. Charact.* **11**(2), 651–659 (2017)
34. R. Khodabakhshian, B. Emadi, M. Khojastehpour, M.R. Golzarian, A. Sazgarnia, Development of a multispectral imaging system for online quality assessment of pomegranate fruit. *Int. J. Food Prop.* **20**(1), 107–118 (2017)
35. M. Soltanikazemi, S. A. Mehdizadeh, M. Heydari, Non-destructive evaluation of the internal fruit quality of black mulberry (*Morus nigra* L.) using visible-infrared spectroscopy and genetic algorithm. *Int. J. Food Prop.* **20**(11), 2437–2447 (2017)
36. N. Sadar, A. Urbanek-Krajnc, T. Unuk, Spectrophotometrically determined pigment contents of intact apple fruits and their relations with quality: a review. *Zemdirbyste-Agric.* **100**(1), 105–111 (2013)
37. M.W. Davey, W. Saeys, E. Hof, H. Ramon, R.L. Swennen, J. Keulemans, Application of visible and near-infrared reflectance spectroscopy (vis/NIRS) to determine carotenoid contents in banana (*Musa* spp.) fruit pulp. *J. Agric. Food Chem.* **57**(5), 1742–1751 (2009)

**Publisher’s Note** Springer Nature remains neutral with regard to jurisdictional claims in published maps and institutional affiliations.

Springer Nature or its licensor (e.g. a society or other partner) holds exclusive rights to this article under a publishing agreement with the author(s) or other rightsholder(s); author self-archiving of the accepted manuscript version of this article is solely governed by the terms of such publishing agreement and applicable law.